

A multi-component reaction (MCR) approach for synthesizing biologically potent tetrazole scaffolds and investigation of their properties using quantum mechanical *ab initio* studies

Ravi Sugandhi^a, Ravi Bansal^a, Gajendra Kumar Inwati^a, Prakash Barfa^a, Rashmi Sharma^b, Pratibha Sharma^a, and Ashok Kumar^{a*}

^aSchool of Chemical Sciences, Devi Ahilya Vishawavidyalaya, Indore, 452001 M.P. - India

^bShri Vaishnav Vidyapeeth vishwavidyalaya, Indore

Email: profpratibhasharma@gmail.com

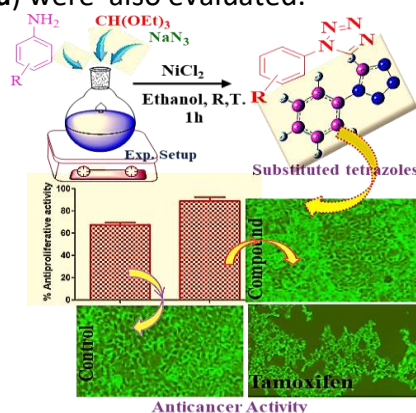
Received 12-26-2024

Accepted 03-31-2025

Published on line 04-20-2025

Abstract

The present investigation elicits the development of a convenient multi-component reaction procedure for synthesizing pharmacologically significant 1-substituted tetrazoles using NiCl_2 in ethanol at room temperature. The excellent yield (up to 94%), ecological compatibility and sustainability factors are the fascinating features of the methodology. The structures of synthesized compounds were accomplished through FT-IR, ^1H -NMR, ^{13}C -NMR, mass, and elemental analysis data. Moreover, computational studies at the B3LYP/6-311G++(d,2p) level of theory were carried out to investigate the energy gap, MEP surface analysis and electron localization function (ELF) of the synthesized compounds. Interestingly, correlation between theoretical and experimental spectral data has also been reported for optimized structures. In addition, anti-cancer and anti-diabetic activities of synthesized compound (**4a**) were also evaluated.



Keywords: Multicomponent synthesis, 1-substituted tetrazoles, DFT calculations, Anti-cancer activity.

Introduction

The chemistry of nitrogen containing heterocycles are widely blossomed in recent times owing to their diversified applicability in various domains including natural products and pharmaceutical chemistry.¹⁻⁵ They have high chemotherapeutic value and act as a prototype for the development of variety of novel drugs.^{6,7} In particular, tetrazoles denote a noteworthy class of heterocyclic compounds⁸ demonstrating their wide utility as antibiotic,⁹ anti-allergic,¹⁰ antagonists,¹¹ antihypertensive,¹² antiviral¹³ antifungal,¹⁴ anti-inflammatory,¹⁵ hormonal¹⁶ and diuretics agents.¹⁷ These compounds have also been used as propellants, explosives, plant growth regulators, herbicides, and fungicides.^{18,19}

Hence, in view of the diversified application associated with tetrazole framework, much attention of organic chemists has been sought to devise synthetic approaches that can lead to develop biologically potential lead compounds embracing this scaffold. A thorough survey of literature eliciting synthetic approaches for construction of tetrazole skeleton utilizes sodium azide, isocyanides cyanides and isocyanates as the synthetic equivalent²⁰. Moreover, many of these procedures have been supported by a number of catalytic systems such as Yb(OTf)₃,^{21,22} In(OTf)₃,²³ [HBim]BF₄,²⁴ SSA,²⁵ natrolite zeolite,²⁷ (Fe₃O₄@AEPH₂-Coll),²⁷ Nd-Schiff-base@BMNPs²⁸ Mg-Al LDH@Guanidine-Cu(II) nanocatalyst²⁹ and Fe₃O₄@SiO₂ nanoparticles.³⁰

However, it was observed that many of these approaches suffer from some serious bottlenecks including the requirement of expensive chemicals, generation of large amount of toxic waste, poisonous and explosive reagents, harsh experimental conditions, excessive amount of catalysts, longer reaction time, tedious work-up procedure, and low yield. Hence, keeping these shortcomings of existing protocols in view, it was thought worth to develop a high-yielding, cost-effective environmentally benign protocol for synthesizing a library of substituted tetrazoles.

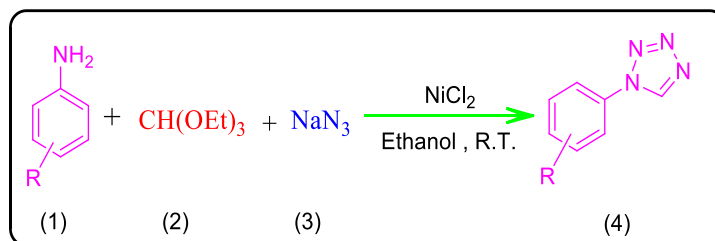
Therefore, encouraged by these findings, in the present study, we describe an efficient strategy in assistance with catalytic support of nickel chloride for synthesizing 1-substituted-1*H*-1,2,3,4-tetrazole derivatives, involving cyclo-condensation reaction among aromatic amine, triethyl orthoformate and sodium azide in ethanolic medium at room temperature (Scheme 1). Also, the density functional theory (DFT) studies were carried out to comprehensively investigate the structural spectral and chemical reactivity parameters of the synthesized tetrazoles.

Results and Discussion

Initially cyclo-condensation reaction among aromatic amines (1 mmol), triethyl orthoformate (1 mmol), and sodium azide (1 mmol),) were carried out in the absence of catalyst in aqueous medium at room temperature, however, no product was resulted even after 24 h (Table 1, entry 1) of the reaction. Further, when the same reaction was carried out in the presence of NiCl₂ (1 mmol) in DMF at room temperature for 24 h, it resulted in 25% yield (Table 1, entry 2) of the product. It was inferred from these observations that thermal conditions are the pre-requisite for the reaction to proceed to some extent. Similarly, when the same reaction was carried out in aqueous conditions using NiCl₂ (0.02 mmol) at 100 °C, gave the 25% yield (Table 1, entry 15) of the product. Furthermore, various catalysts were also tried, but the results were not encouraging, (Table 1, entries 3–13). Interestingly, 94% yield of the product (Table 1, entry 14), was obtained when the reaction was carried out in ethanolic medium at room temperature, using NiCl₂ (0.2mmol) as catalyst for 1 h time. A comparative account of all these findings is depicted in Table 1.

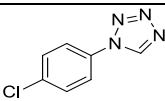
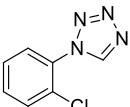
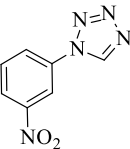
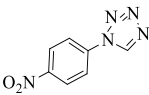
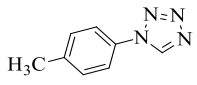
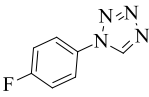
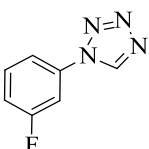
Table 1. Effects of different catalyst and solvent on the reaction

Entry	Catalyst	Solvent	Time (h)	Temp. (°C)	Yield (%)
1	-----	Water	24	r.t.	No product
2	NiCl ₂	DMF	24	r.t.	25
3	-----	Ethanol	24	r.t.	30
4	ZnCl ₂	Ethanol	24	80	30
5	Al ₂ O ₃	Ethanol	8	60	30
6	TEA	DMF	24	100	Trace
7	CuO	DMF	14	60	Trace
8	ZnO	THF	24	r.t.	30
9	CuCl ₂	THF	10	80	30
10	Fe ₂ O ₃	Ethanol	24	70	No product
11	TEA	THF	24	r.t.	25
12	TEA	Ethanol	24	70	25
13	TEA	THF	6	100	25
14	NiCl ₂	Ethanol	1	r.t.	94
15	NiCl ₂	water	24	100	25
16	NiCl ₂	----	24	r.t	No product

Table 2. Library of Synthesis of 1-substituted-1*H*-1,2,3,4-tetrazole

Entry	Aromatic amine (R)	Product	Time(h)	Yield %	M.P. (°C)
1.	H		1	94	63-64
2.	3- Cl		1	85	152-154
3.	4-Br		1	85	168-170

Table 2. Continued

Entry	Aromatic amine (R)	Product	Time(h)	Yield %	M.P. (°C)
4.	4-Cl	 4d	1	87	152-154
5.	2-Cl	 4e	1.5	85	142-144
6.	3-NO ₂	 4f	1.5	90	200-201
7.	4-NO ₂	 4g	1	80	200-201
8.	4-CH ₃	 4h	1.5	81	91-101
9.	4-F	 4i	1	86	180-182
10.	3-F	 4j	1.5	90	175-177

Reaction conditions : aromatic amine (1 mmol), triethyl orthoformate (1 mmol), sodium azide (1 mmol), NiCl₂ (0.02 mmol) as catalysts, in ethanol at room temperature.

Additionally, the effect of catalytic amount on the rate of the reaction was also studied using various concentrations of the catalyst (Table 3) under similar conditions. The highest yield (94 %) was obtained with 0.02 mmol of NiCl₂.

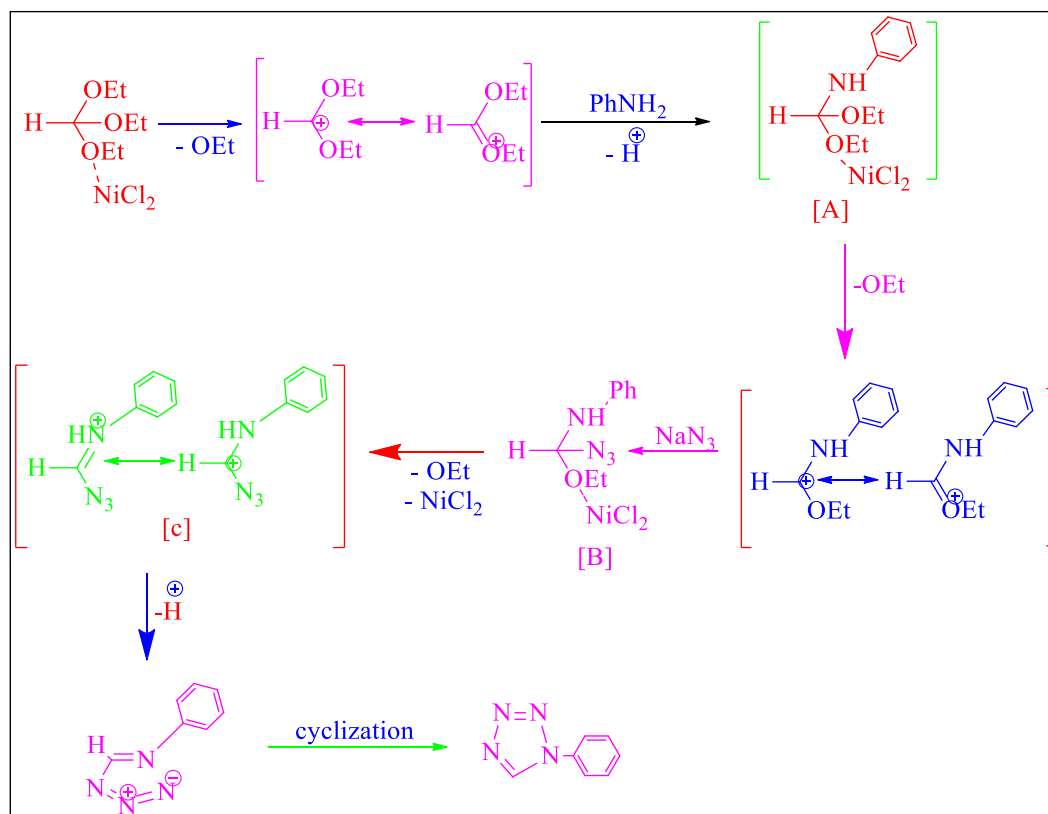
Table 3. Effects of catalytic amount of NiCl₂ on the product at room temperature

Entry	NiCl ₂ (mmol)	Yield (%)
1	0.005	20
2	0.01	30
3	0.02	94
4	0.03	20
5	0.04	10
6	0.12	20

Reaction conditions : Triethyl orthoformate (1 mmol), aromatic amine, (1 mmol), sodium azide (1 mmol) NiCl₂ (0.02 mmol) as catalysts, in ethanol at room temperature.

2.1. Plausible mechanism

The proposed mechanism for the synthesis of 1*H*-1,2,3,4-tetrazoles derivatives through a multicomponent reaction (MCR), catalyzed by NiCl₂ is illustrated in Scheme 2. The role of NiCl₂ was to activate the ethoxy group of triethyl orthoformate, cleaving C–O bonds to give carbenium ion. The sequential nucleophilic displacement by amine and azide anions generate intermediates **A** and **B**. At this point, NiCl₂ assisted in elimination of ethanol from **B**, leading to the formation of intermediate **C**, which upon cyclization yields the final product.²³

**Scheme 2.** Proposed reaction mechanism for the synthesis of 1*H*-1,2,3,4-tetrazoles.

Computational studies

The optimized molecular structure with minimum energy was obtained through Gaussian 09 and Gauss view 6.0 software.³¹⁻³³ The geometry was optimized by B3LYP/6-311++ G(d,2p) basis set. Various molecular properties such as HOMO-LUMO energy, MEP surface analysis, atoms in molecule (AIM) theory has been utilized to calculate electrophilicity index, electron density, and electron localization function (ELF) of the synthesized compounds and the results were plotted.

Optimized molecular geometry. The optimized geometrical parameters of the least energy in terms of bond length and bond angles are shown in Table 4 and Figure 1. The experimental results were compared with the optimized geometry of the compound (**4a**) derived by DFT/B3LYP using 6-311++G(d,2p) and Hartree-fock Method³⁴ B3LYP, which was used in the optimization process to identify the best data which agreed with the experimental values. The data acquired by B3LYP with 6-311++G(d,2p) is the best match with experimental data. We can see from Table 4 that there is a tiny discrepancy between the theoretical and experimental values which is due to the fact that the experimental calculations were conducted in a solid phase and, theoretical calculations were conducted in the gas phase. The picture of the optimized geometric structure with marked atoms is presented in Table 5.

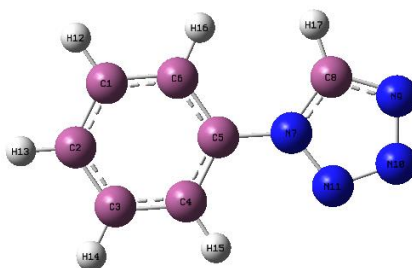


Figure 1. Optimized molecular geometrical structure with atom numbering of 1-phenyl-1*H*-tetrazole: all nitrogen shown by blue, carbon by grey, hydrogen by white color.

Table 5. Optimized geometry of the synthesized 1-substituted-1*H*-1,2,3,4-tetrazoles

S. No.	Structure	Optimized Geometry
1.	<p>4a</p>	
2.	<p>4b</p>	

Table 5. Continued

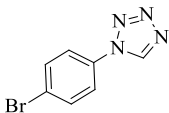
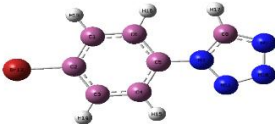
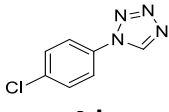
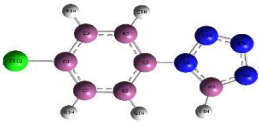
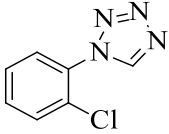
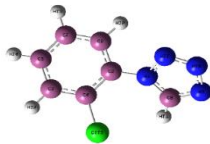
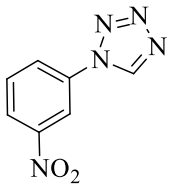
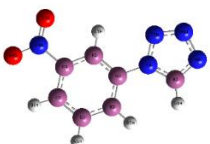
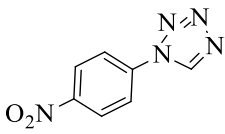
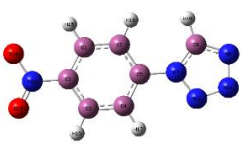
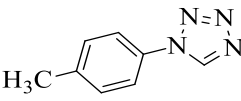
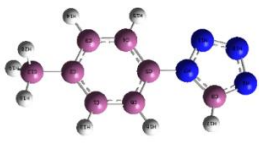
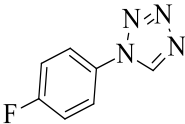

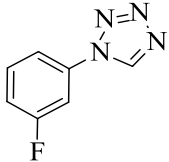
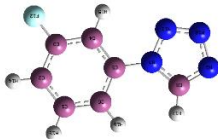
S. No.	Structure	Optimized Geometry
3.	 4c	
4.	 4d	
5.	 4e	
6.	 4f	
7.	 4g	
8.	 4h	

Table 5. Continued

S. No.	Structure	Optimized Geometry
9.	 <p style="text-align: center;">4i</p>	
10.	 <p style="text-align: center;">4j</p>	

Frontier molecular orbital (FMO). The evaluation of frontier molecular orbitals of the compounds is a significant study in drug design in recognizing their reactivity.³⁵⁻³⁷ The highest occupied molecular orbital (HOMO) and the lowest unoccupied molecular orbital (LUMO) of the synthesized 1-substituted-1*H*-1,2,3,4-tetrazoles are shown in Figure 2, and Figure 3. HOMO is the electron donor orbital which shows how much tendency a molecule may have to transfer an electron whereas LUMO is the electron acceptor orbital, which shows how much capacity a molecule can have to accept an electron. The HOMO- LUMO energy gap between of the synthesized compounds (**4a-j**) are shown in Figure 4 which is crucial for charge transfer interaction (CTI) or electron transition (ET) activities. From the results, the maximum energy gap is observed in the compound **4e** (-5.7494 eV), therefore, the charge transfer interaction or electron transition (ET) CTI/ET is expected to be difficult in it. The compound **4g** have lowest energy gap i.e., -4.6520 eV; there by the charge transfer interaction (CTI) or electron transition (ET) activities were expected to undergo easily.

Many other significant variables such as ionization potential (I.E), electrophilicity index (ω), chemical Potential [μ], chemical hardness (η), electron affinity (E.A) and dipole moment were calculated using Koopman's theorem,³⁸⁻⁴⁴ providing information about the electronic properties and reactivity of the molecules. The compound **4g** exhibits the maximum electrophilicity index value (7.2679), may be due to the interaction with the nucleophilic species, while the lowest electrophilicity index value (3.7724) is obtained for the compound **4h**. Likewise, compound **4e** demonstrates the highest negative value (-2.8747) for chemical hardness, indicating its heightened stability and reduced susceptibility to decomposition into constituent elements. These findings are summarized in Table 6.

Table 6. Calculated the quantum mechanical parameters for 1-substituted-1H-1,2,3,4-tetrazole derivatives

Comp.	E _{HOMO} (eV)	E _{LUMO} (eV)	$\Delta E_{(HOMO-LUMO)}$ (eV)	η (eV)	μ (eV)	ω (eV)	Dipole moment μ (Debye)
4a	-7.4062	-1.9434	-5.4628	-2.7314	-4.6748	4.0004	6.5598
4b	-7.5382	-2.1864	-5.3518	-2.6759	-4.8623	4.4175	6.3458
4c	-7.2691	-2.1768	-5.0923	-2.5461	-4.7229	4.3803	5.0900
4d	-7.3453	-2.1572	-5.1881	-2.5940	-4.7610	4.3691	5.0079
4e	-7.5948	-1.8454	-5.7494	-2.8747	-4.7201	4.0516	6.6474
4f	-8.0819	-3.4008	-4.6811	-2.3405	-5.7413	7.0417	7.0645
4g	-8.1407	-3.4887	-4.6520	-2.3260	-5.8147	7.2679	1.8500
4h	-7.1183	-1.8234	-5.2949	-2.6474	-4.4708	3.7724	7.1538
4i	-7.4207	-2.0310	-5.3897	-2.6948	-4.7258	4.1437	4.9428
4j	-7.6081	-2.1741	-5.4340	-2.7170	-4.8911	4.4024	6.3701

Values highlighted in bold represents the highest and lowest values of each quantum mechanical parameter

Molecular electrical potential (MEP) surface. Molecular electrical potential surface was employed to evaluate the physicochemical properties of the synthesized compounds in 3D surface.⁴⁵ The method evaluates the charged area of the synthesized compound in a view to determine the molecular interaction and the nature of the chemical bonds. Significantly, it shows the molecular size, shape, negative, positive, and neutral electrostatic potential through colour marking.

The MEP surface envisaging the reactive sites in the optimized structure of all of the synthesized compounds **4(a-j)** is mapped as shown in Figure 5. In this visualization the increasing order of electrostatic potential is found in the order of red < brick red < green < blue. The red color in the map signifies an electronegative region with minimum electrostatic potential that divulges its susceptibility to electrophilic attack. Conversely, the blue color signifies an electropositive region liable for the nucleophilic attack, while green is a region of zero potential.^{46,47}

Analysis of the MEP diagrams revealed that the red colour exhibited an electrophilic attack over the nitrogen atom of the tetrazole ring and green display the chlorine atom, whereas the brick red color indicates the bromine atom. In our target molecule red region displays the corresponding oxygen atom of the nitro group, which is the most reactivity toward the intramolecular hydrogen bonding.

Electron localization function (ELF). ELF analysis offers evidence about the data of the chemical structure, molecular bonding reactivity, and quantitative analysis of the aromaticity of the compound. It gives information of electron pair with opposite spin's and also estimates the spatial localization or delocalization of the reference electron. The value of ELF is based on Pauli's repulsion. If the value of ELF is one then that region is called the maximum Pauli repulsion region and is represented by red color whereas if the value of ELF is zero or near zero then the region is called the minimum Pauling repulsion region which is denoted by blue color. The compound's C5, C6, and C7 atoms were selected in a single plane, as seen in Figure 6. The high value of ELF was represented by red colour, the middle ELF value expressed as yellow to green colour and the lowest value of ELF is shown by blue color.

In the titled molecule, it is observed that the C-C and C-N covalent bonds have maximum LOL value and maximum degree of ELF in that region. The blue ring region signifies valence and the inner shell of heavy nucleus. As a result of the hydrogen and carbon atoms' repulsion, the density was lower in the space between

the C-H bonds. The huge changes from yellow to green for medium ELF values of 0.7 and lower ends, as shown by blue, while high ELF values were red in colored 1.4–1.0. Basis of measurement in ELF diagram is Pauli repulsion, ELF value ranges from 0 to 1. When ELF is 1, that is the area of maximum Pauli repulsion, and electrons were well localized, similarly when ELF is 0, that region is of minimum Pauli repulsion and electrons were delocalized in this region.^{48,49}

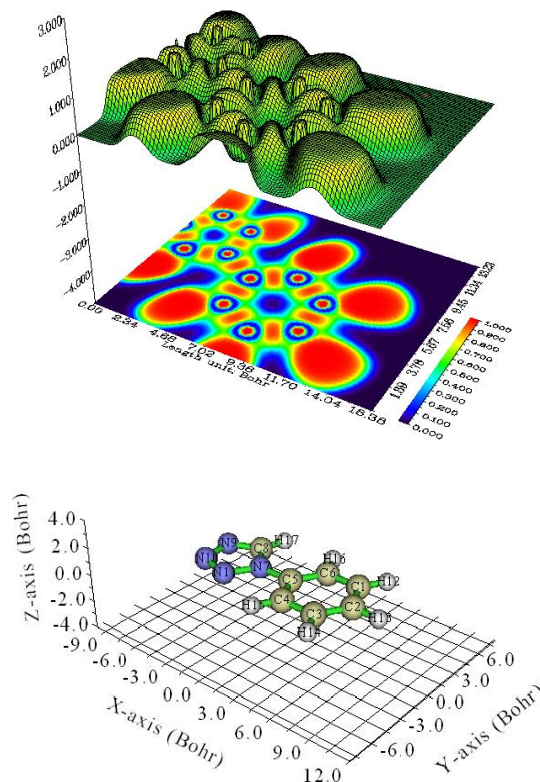


Figure 6. ELF (A) Color filled map and (B) Shaded surface map with projection effect of hydrogen bonding region in 1-substituted-1*H*-1,2,3,4-tetrazoles.

NMR analysis. The theoretical ^{13}C -NMR and H-NMR spectral data of compound (4a) were calculated in methanol using Gaussian 09 and 1 Gauss view 6.0 software²⁷ at the B3LYP level with 6–311++G (d,2p) basis set. Experimental and computed chemical shifts are listed in Table 7.

In the experimental ^1H -NMR spectrum (Figure 7), chemical shifts at δ 10.69, 7.50, 7.48, 7.25, 7.01, and 7.13 were observed for synthesized compound **4a**, while corresponding theoretical values (ppm) are illustrated in the simulated spectra (Figure 8). Minor discrepancies between the NMR values of experimental and theoretical peaks are attributed to solvent effects. Similarly, the simulated ^{13}C -NMR experimental chemical shifts (Figure 9) for carbon atoms C1, C2, C3, C4, C5, C6, and C8 were found to be 137.0, 129.3, 129.5, 129.2, 145.1, 128.9 and 149.8 ppm, respectively. Corresponding theoretical values are assigned as, 135.1, 134.0, 135.1, 124.0, 140.0, 122.0, and 144.0 ppm (Figure 10) respectively.

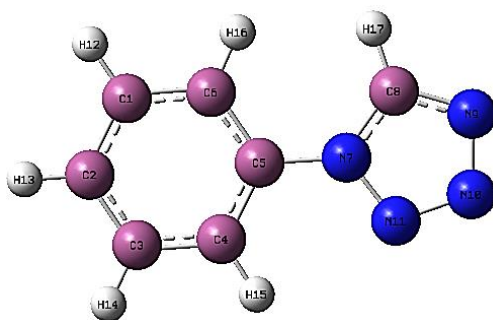


Figure 1. Optimized molecular geometrical structure with atom numbering of compound (**4a**).

Table 7. ^1H -NMR and ^{13}C -NMR data experimental and theoretical values of compound **4a** in ppm

S. NO.	^1H -NMR	DFT(B3LYP)	Expérimental	^{13}C -NMR	DFT(B3LYP)	Expérimental
1.	17-H	9.61	10.69	1-C	135.1	137.0
2.	16-H	8.20	7.50	2-C	134.0	129.3
3.	15-H	8.49	7.48	3-C	135.1	129.5
4.	14-H	8.01	7.47	4-C	124.0	129.2
5.	13-H	7.09	7.04	5-C	140.0	145.1
6.	12-H	8.10	7.24	6-C	122.0	128.9
7.				8-C	144.0	149.8

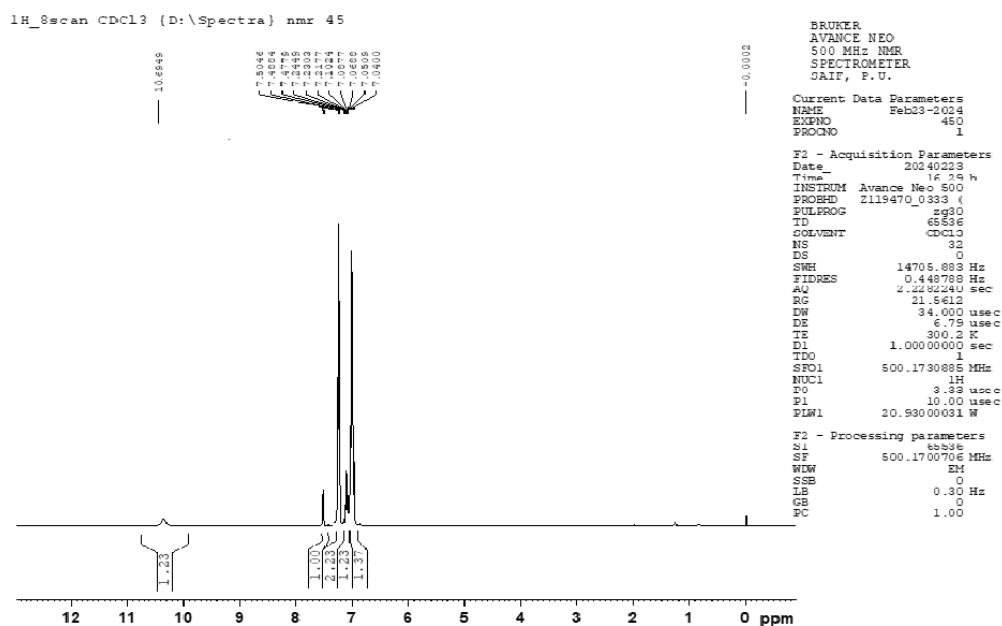


Figure 7. ^1H -NMR Expérimental spectra of 1-phenyl-1H-tetrazole (**4a**).

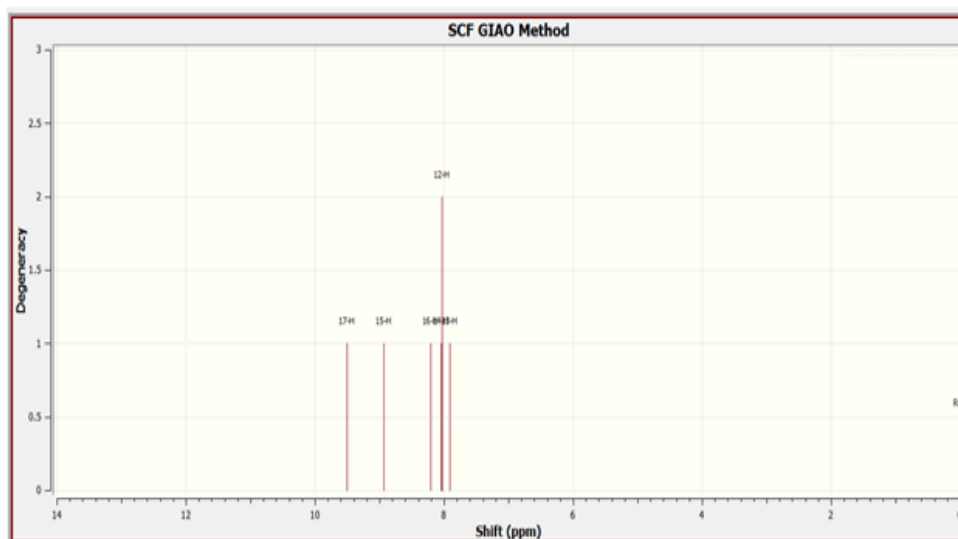


Figure 8. Theoretical ^1H -NMR spectra of compound (4a).

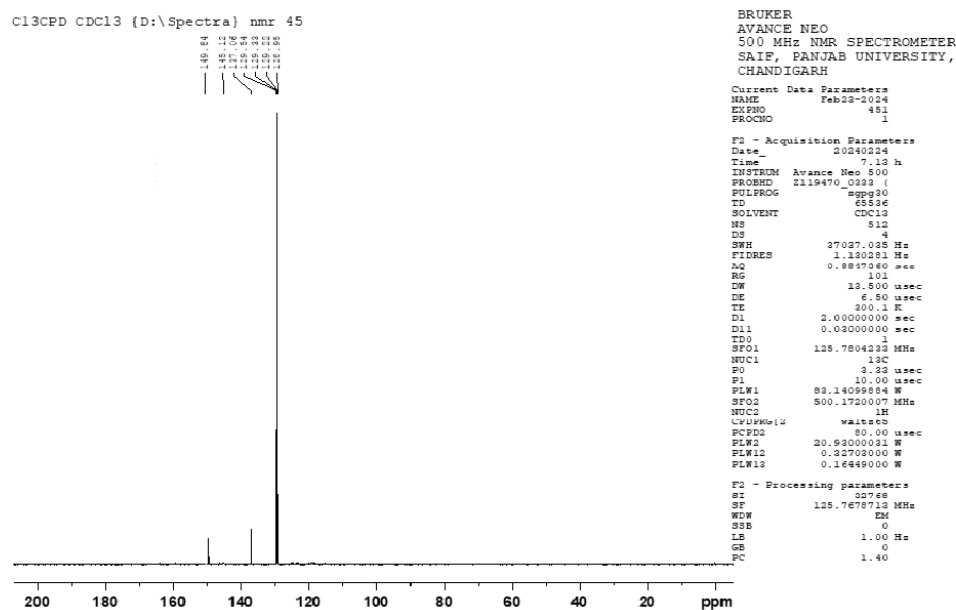


Figure 9. ^{13}C -NMR Experimental spectra of 1-phenyl-1H-tetrazole (4a).

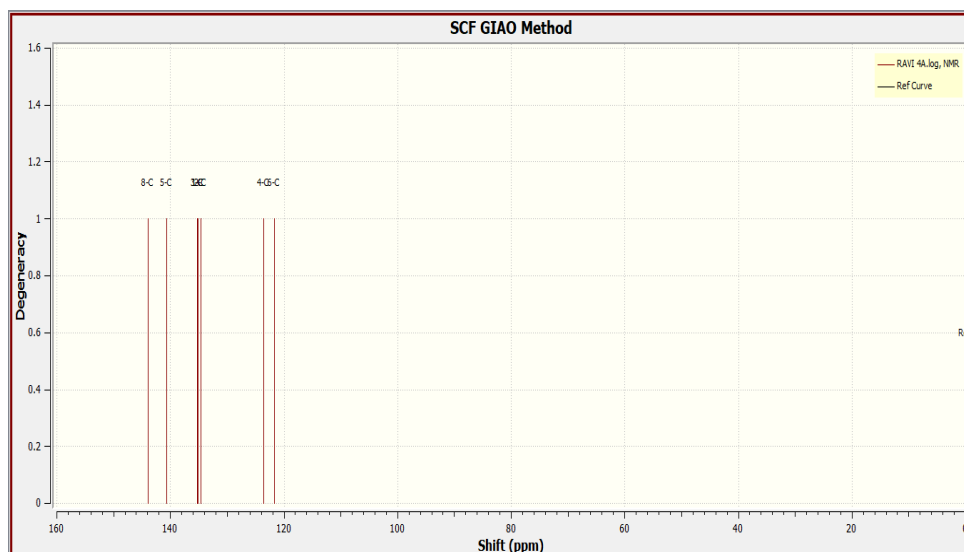


Figure 10. Theoretical ^{13}C -NMR Spectra of compound (**4a**).

Conclusions

An efficient and environmentally benign protocol has been developed for the synthesis of biologically important 1-substituted tetrazoles involving multi-component reaction strategy assisted by catalytic influence of NiCl_2 in ethanol at room temperature. This methodology is amenable to multigram-scale production, rendering it economically viable for large-scale preparation.

The operational simplicity, high purity of the products, ability to isolate products without chromatographic purification, and utilization of eco-friendly catalysts could pave the way for both academic research and practical applications. Also, DFT analysis corroborates these findings, elucidating the molecular structure and properties of the synthesized compounds. Moreover, the synthesized compound 1-phenyl-1H-tetrazole indicated their potential to be used as an anticancer and anti-diabetic drug.

Experimental Section

General. All chemical reagents and solvents were purchased from Merck and Sigma-Aldrich chemical companies and utilized without further purification. The melting points of compounds were determined using a vego melting point apparatus and remained uncorrected. Fourier-transform infrared (FTIR) spectra were acquired in the range of $400\text{--}4000\text{ cm}^{-1}$ utilizing a Perkin Elmer Spectrum IR version 10.7.2 spectrometer. The purity determinations of the products were accomplished by TLC on silica gel polygram STL G/UV 254 plates. The spectra were recorded employing a Bruker Advance Neo spectrometer at frequencies of 500 MHz (^1H -NMR) and 125 MHz (^{13}C -NMR), with $\text{DMSO-}d_6$ as the solvent and tetramethylsilane as the internal standard. All the yields refer to isolated products after purification by thin-layer chromatography or recrystallization.

General synthesis for the preparation of 1H-1,2,3,4-tetrazoles. A mixture of triethyl orthoformate (1.2 mmol), sodium azide (1 mmol), and aromatic amine (1 mmol) were taken in a 100 ml round-bottomed flask and stirred at room temperature for the duration specified in Table 2. The progress of the reaction was monitored

by thin-layer chromatography (TLC) using an ethyl acetate and *n*-hexane (3:7) mixture as the mobile phase. After completion of the reaction, the mixture was filtered, and the filtrate was washed with distilled water to remove the catalyst. The resulting solid was isolated by suction filtration to afford the crude product, which was further purified by recrystallization from ethyl acetate to yield the crystalline pure product.

1-Phenyl-1H-tetrazole (4a). White solid (94% yield); mp: 63-64 °C. ¹H NMR (500 MHz, DMSO-*d*₆): 10.69 (s, 1H), 7.50 (t, 1H, *J* 08 Hz, Ar-H), 7.21 (t, 1H *J* 08 Hz, Ar-H) 7.05 (t, 1H, *J* 08Hz, Ar-H), 7.08 (d, 2H, *J* 7.5 Hz, Ar-H) ppm. ¹³C NMR (125 MHz, DMSO-*d*₆): 149.8, 145.1, 137.0, 139.5, 129.3, 129.2, 128.9 ppm. MS (ESI mass) *m/z* [M+H]⁺: 146.16; FTIR (cm⁻¹): 3070 (=CH, sp²), 2883 (-CH, sp³), 1679 (N=N), 1536, (C=C), 1478, 1421, 1311 1095, 871 (C=C Str. Ar). Analytical Calculated Formula C₇H₆N₄: C, 57.53; H, 4.14; N, 38.34; Found: C, 57.45; H, 4.10; N, 38.28.

1-(3-Nitrophenyl)-1H-tetrazole (4b). Gray White solid (90% yield); mp:152-154 °C. ¹H NMR (500 MHz, DMSO-*d*₆): 10.02 (s, 1H), 8.69 (s, 1H, Ar-H), 7.36 (t, 1H, *J* 08 Hz, Ar-H), 7.14 (d, 1H, *J* 08 Hz, Ar-H) 7.05 (t, 1H, *J* 08 Hz, Ar-H), ppm. ¹³C NMR (125 MHz, DMSO-*d*₆): 153. 3, 147.6, 130.4, 130.2, 130.0, 125.2, 124.8 ppm. FTIR (cm⁻¹): 3063(=CH, sp²), 2927(-CH, sp³), 1666, (N=N), 1583, (C=C), 1484, 1387, 1203, 1088, 827 (C=C Str. Ar), cm⁻¹. Analytical Calculated Formula C₇H₅ClN₄: C, 46.55; H, 2.79; Cl, 19.63, N, 31.02; Found: C, 46.45; H, 2.70; Cl, 19.53; N, 31.00.

1-(4-Bromophenyl)-1H-tetrazole (4c). Brown solid (90% yield); mp:168-170 °C. ¹H NMR (500 MHz, DMSO-*d*₆): 10.35 (s, 1H), 7.50 (dd, 2H, *J* 08 Hz, Ar-H), 7.43 (dd, 2H, *J* 7.5 Hz, Ar-H), ppm. ¹³C NMR (125 MHz, DMSO-*d*₆): 159.5, 148.0, 131.7, 131.5, 131.3, 120.9, 119.2 ppm. FTIR (cm⁻¹): 3093 (=CH, sp²), 2926 (-CH, sp³), 1621 (N=N), 1521(C=C), 1485, 1389, 1345, 1086, 867(C=C Aromatic stretching). Analytical Calculated Formula C₇H₅BrN₄: C, 37.36; H, 2.24; Br, 35.51, N, 24.90; Found: C, 37.30; H, 2.20; Br, 35.41; N, 24.80.

1-(4-Chlorophenyl)-1H-tetrazole (4d). White solid (90% yield); mp:152-154 °C. ¹H NMR (500 MHz, DMSO-*d*₆): 9.93 (s, 1H), 7.40 (dd, 2H, *J* 08 Hz, Ar-H), 7.37 (dd, 2H, *J* 7.5 Hz, Ar-H), ppm. ¹³C NMR (125 MHz, DMSO-*d*₆): 159.4, 148.1, 137.0, 129.0, 128.8, 128.6, 128.4 ppm. FTIR (cm⁻¹): 3163(=CH, sp²), 2932 (-CH, sp³), 1652, (N=N), 1592(C=C), 1386, 1314, 1113, 870 (C=C Str. Ar). Analytical Calculated Formula C₇H₅ClN₄: C, 46.55; H, 2.79; Cl, 19.63, N, 31.02; Found: C, 46.45; H, 2.70; Cl, 19.53; N, 31.00.

1-(2-Chlorophenyl)-1H-tetrazole (4e). White solid (90% yield); mp:142-144 °C. ¹H NMR (500 MHz, DMSO-*d*₆): 9.28 (s, 1H), 7.47 (d, 1H, *J* 7.5 Hz, Ar-H), 7.45 (d, 1H, *J* 7.5 Hz, Ar-H), 7.32 (t, 1H, *J* 08 Hz, Ar-H), 7.05 (t, 1H, *J* 08 Hz, Ar-H), ppm. ¹³C NMR (125 MHz, DMSO-*d*₆): 160.2, 149.0, 129.2, 128.8, 127.7, 127.4, 127.2 ppm. FT-IR (KBr) (cm⁻¹) 3062(=CH, sp²), 2867(-CH, sp³), 1665(N=N), 1584(C=C), 1471, 1386, 1311, 1054, 864 (C=C Str. Ar). Analytical Calculated Formula C₇H₅ClN₄: C, 46.55; H, 2.79; Cl, 19.63, N, 31.02; Found: C, 46.45; H, 2.70; Cl, 19.53; N, 31.00.

1-(3-Nitrohenyl)-1H-tetrazole (4f). Yellow solid (90% yield); mp: 200-201 °C. ¹H NMR (500 MHz, DMSO-*d*₆): 10.49 (s, 1H), 8.58 (s, 1H, Ar-H), 7.51 (d, 1H, *J* 07 Hz, Ar-H), 7.40 (d, 1H *J* 08 Hz, Ar-H), 7.29 (t, 1H *J* 7.5 Hz, Ar-H) ppm. ¹³C NMR (125 MHz, DMSO-*d*₆): 160.8, 148.6, 130.1, 128.9, 123.2, 120.9, 119.8 ppm. FT-IR (KBr) (cm⁻¹): 3149 (=CH, sp²), 2926(-CH, sp³), 1650(N=N), 1592 (C=C), 1386, 1114, 777 (C=C Str. Ar). Analytical Calculated Formula C₇H₅N₅O₂: C, 43.98; H, 2.64; N, 36.64. Found: C, 43.90; H, 2.60; N, 36.54.

Evaluation of anticancer activity

The compound 4a was subjected to in-vitro anticancer activity assay against human liver cancer cell line (HepG2), using MTT assay (Figure 11). An appropriate positive control was run in each experiment and was repeated thrice. The compound 4a inhibited the growth of HepG2 cells at IC 50 (concentration of compound causing 50% inhibition of cell growth) of less than 50.0 μM.

Cell lines and culture

The National Centre for Cell Science (NCCS), Pune, India provided the human liver cancer cell line (HepG2), which was cultured. The cell lines were kept in ambient condition in an incubator with 5% CO₂ and 37 °C. They were further supplemented with 10% fetal bovine serum, 100 U/ml penicillin, and 100 mg/ml streptomycin in Dulbecco's modified Eagle medium.

Antiproliferative assay

Cell proliferation inhibition was investigated according to a previously reported protocol with minor modifications.⁵⁰⁻⁵⁵ HepG-2 cells were used for the 3-(4, 5-dimethylthiazol-2-yl)-2, 5-diphenyltetrazolium bromide (MTT) test in accordance with established procedures. A 96-well plate was used for cell plating, with 5,000–7,000 cells per well. Fresh medium was added to the cells, and an aqueous extract that had been refrigerated for the previous night using a rotary shaker was added. Each well received 20 µl of MTT dye (5 mg/ml) after 24 hours, and then there was a 4-hr incubation period. Formazon crystal precipitates were dissolved in 200 µl of dimethyl sulfoxide (DMSO) for fifteen minutes on a shaker. Following the addition of MTT dye, every step was carried out in the dark. At 550 nm, absorbance was measured. Tamoxifen was the typical anticancer medication. The % cell inhibition was calculated using the following formula:

Cell proliferation inhibition (%) = $[1 - (A_s/A_c)] \times 100$ where: A_s – absorbance of sample; A_c – absorbance of control.

Antiproliferative effects of compound 4a on the HepG2 cancer cells

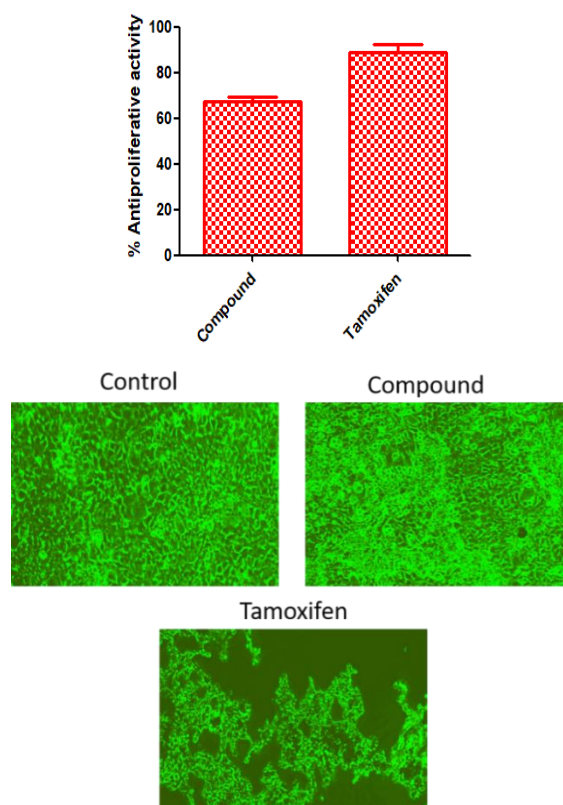


Figure 11. Morphological changes (Magnification 10X) in HepG2 cell line after treating with synthesized compound (4a).

The selection of HepG2 cancer cell lines was based on the persistence of numerous desirable characteristics. Although the liver is the body's primary organ for detoxification and mostly in control of drug metabolism and drug-drug interactions, hepatic cells play a significant role in the drug discovery process. HepG2 cells are therefore often employed in toxicity testing and drug development.

Using the MTT evaluation, the antiproliferative effect of multiple extracts on HepG2 cell lines was established. The compound antiproliferative values were tested against tamoxifen, a positive anticancer medication. After 24 h treatment, HepG2 cancer cells revealed antiproliferative activity with value of $67.25 \pm 2.7 \%$ for compound 4a that was comparable to standard drug ($88.8 \pm 5.2 \%$).

Determination of antidiabetic activity- α -Glucosidase inhibition assay

The α -glucosidase inhibitory activity was determined as per the protocol of Yu *et al.*⁵⁶ with slight modifications. The enzyme α -glucosidase reacts with the substrate p-nitrophenyl- α -D-glucopyranoside (pNPG) and releases p-nitrophenol (pNP) which can be measured at 405 nm. Compound (4a) was pre-incubated with 1 ml of α -glucosidase (1 U/ml) in 0.1 M phosphate buffer (pH 6.9) at 25°C for 10 min. To this, 1 ml of 5 mM pNPG was added and incubated at 25°C for 10 min. Then, 2 ml of Na_2CO_3 was added to terminate the reaction before reading the absorbance at 405 nm. Acarbose was used as positive control. The results of α -glucosidase inhibition was expressed as inhibition percentage as given under;

$$\text{Inhibition \%} = ((A_{\text{control}} - A_{\text{sample}}) / A_{\text{control}}) \times 100\%$$

α -Glucosidase Inhibitory Activity

α -glucosidase is another key enzyme involved in starch digestion that breaks terminal α -1 to 4-linked glucose releasing a single glucose molecule that can be absorbed by the body. The assay for α -glucosidase inhibitory activity of compound (4a) was measurable with IC_{50} $92.7 \pm 1.44 \mu\text{g/ml}$ in comparison to acarbose (IC_{50} value $55.12 \pm 2.35 \mu\text{g/ml}$). This suggests that compound have the potential to be developed into functional ingredients for diabetic care.

Acknowledgements

The authors are thankful to the School of Chemical Sciences, Devi Ahilya University, Indore (M.P.) for providing facilities and resources. The authors are grateful to SAIF, Chandigarh, and CDRI, Lucknow for the characterization of products. The authors are grateful to the School of Studies in Biotechnology, Jiwaji University, Gwalior (M.P.) for providing the biological facilities for the synthesized compound.

Supplementary Material

Supporting Information File: Compound characterization data (FTIR, ^1H , ^{13}C NMR and Computational Studies) of synthesized compounds.

References

1. Anthony, J. E.; Chem. Rev. **2006**, *106*, 5028-5048.
<https://doi.org/10.1021/cr050966z>
2. McGrath, N. A.; Brichacek M.; Njardarson, J. T. J. Chem. Edu. **2010**, *10*, 1348-1348.

- <https://doi.org/10.1021/ed1003806>.
3. Yang, X.; Zhou, G.; Wong, W.Y.; Chem. Soc. Rev. **2015**, 44, 8484-8575.
<https://doi.org/10.1039/C5CS00424A>
 4. Delfourne, E. Bastide, J. Med. Res. **2003**, 23, 234-252.
<https://doi.org/10.1002/med.10032>
 5. Jacobs, L.; de Kock, C.; Taylor, D.; Pelly S. C.; Blackie, M. A. L.; Bioorg. Med. Chem. **2018**, 26, 5730- 5741.
<https://doi.org/10.1016/j.bmc.2018.10.029>.
 6. Brahmabhatt, H.; Molnar, M.; Pavić, V. K. Int. J. Mod. Sci. **2018**, 4, 200206.
<https://doi.org/10.1016/j.kijoms.2018.01.006>.
 7. Reyes-Arellano, A.; Gómez-García, O.; Torres-Jaramillo, J. Med. Chem. **2016**, 6, 561-570.
<https://doi.org/10.4172/2161-0444.1000400>.
 8. Rees, A. R.; Scriven, C.W.; Eds, E.F.V. Pergamon. 1996, 4, 621-678.
<https://doi.org/10.4236/ijoc.2015.52009>.
 9. Andrus, A.; Partridge, B.; Heck, J. V.; Christensen, B. G. Tetrahedron Lett. **1984**, 25, 911-914.
[https://doi.org/10.1016/S0040-4039\(01\)80060-5](https://doi.org/10.1016/S0040-4039(01)80060-5).
 10. Peet, N. P.; Baugh, L. E.; Sunder, S.; Lewis, J. E.; Matthews, E.; Holberding, E. L.; Shah, D. N. J. Med. Chem. **1986**, 29, 2403-2409.
<https://doi.org/10.1021/jm00161a045>.
 11. Castro, J. L.; Ball, R. G.; Broughton, H. B.; Russell, M. G. N.; Rathbone, D.; Watt, A. P.; Baker, R.; Chapman, K. L.; Fletcher, A. E.; Smith, A. J.; Marshal, G. R.; Ryecroft W.; Matassa, V. G. J. Med. Chem. **1996**, 39, 842-849.
<https://doi.org/10.1021/jm00072a005>
 12. Wexler, R.R.; Greenlee, W.J.; Irvin, J.D.; Goldberg, M.R.; Prendergast, K.; Smith, R.D.; Timmermans, P.B. M. W. M. J. Med. Chem. **1996**, 39, 625-656.
<https://doi.org/10.1021/jm9504722>.
 13. Wittenberger, S.J.; Org. Prep. Proced. Int. **1994**, 26, 499-531.
<https://doi.org/10.1080/00304949409458050>.
 14. Ahmad Malik, M.; Al-Thabaiti, S. A.; Malik, M.A. Int. J. Mol. Sci. **2012**, 13, 10880- 10898.
<https://doi.org/10.3390/ijms130910880>.
 15. Bepary, S.; Das, B.; Bachar, S.C. K.; Kundu, J.K.; Shamsur rouf, A.S.; Datta B.K.; Pak. J. Pharm. Sci. **2008**, 21, 295-298.
<https://doi.org/10.13140/2.1.3745.8884>.
 16. Li, J.; Chen, S.Y.; Tao, S.; Wang, H.; Li, J. J.; Swartz, S.; Musial, C.; Hernandez, A. A.; Flynn, N.; Murphy, B.J.; Beehler, B.; Dickinson, K.E.; Giupponi, L.; Grover, G.; Seethala, R.; Sleph, P.; Slusarchyk, D.; Yan, M.; Humphreys, W.G.; Zhang, H.; Ewing, W. R.; Robl, J.A.; Gordon, D.; Tino, J. A. Bioorg. Med. Chem. Lett. **2008**, 18(6), 1825-1829.
<https://doi.org/10.1016/j.bmcl.2008.12.093>
 17. Nachman, R.J.; Coast, G.M.; Kaczmarek, K.; Williams, H. J.; Zabrocki, J. Acta. Biochim. Pol. **2004**, 51, 121-127.
https://doi.org/10.18388/abp.2004_3603.
 18. Ostrovskii, V. A.; Pevzner, M.S.; Kofmna, T.P.; Shcherbinin, M.B.; Tselinskii, I. V. Targets Heterocycl. Syst. 3, **1999**, 467-526.
<https://doi.org/10.1002/CHIN.200050296>.
 19. Jursic, B.S.; Leblanc, B.W. J. Heterocycl. Chem. **1998**, 35, 405-408.

- <https://doi.org/10.1002/jhet.5570350224>.
20. Pokhodylo, N.T.; Matiyshuk, V.S.; Obushak, M.D. *Tetrahedron* **2008**, *64*, 1430-1434.
<https://doi.org/10.1016/j.tet.2007.11.045>.
21. Gupta, A.K.; Song, C.H.; Chang, H.O. *Tetrahedron Lett.* **2004**, *45*, 4113-4116.
<https://doi.org/10.1016/j.tetlet.2004.03.162>.
22. Su, W.; Hong, Z.; Shan, W.; Zhang, X. *Eur. J. Org. Chem.* **2006**, 2006(12), 2723-2726.
<https://doi.org/10.1002/ejoc.200600007>.
23. Dhiman, K.; Adinath, M.; Alakananda, H. *Tetrahedron Lett.* **2009**, *50*, 2668-2670.
<https://doi.org/10.1016/j.tetlet.2009.03.131>.
24. Potewar, T.M.; Siddiqui, S.A.; Lahoti, R.J.; Srinivasan, K.V. *Tetrahedron Lett.* **2007**, *48*, 1721-1724.
<https://doi.org/10.1016/j.tetlet.2007.01.050>.
25. Habibi, D.; Nabavi, H.; Nasrollahzadeh, M. *Journal of Chem.* **2012**, 1-4.
<https://doi.org/10.1155/2013/645313>.
26. Habibi, D.; Nasrollahzadeh, M.; Kamali, T.A. *Green Chem.* **2011**, *13*, 3499-3504.
<https://doi.org/10.1039/C1GC15245A>.
27. Salimi, M.; Nasrabadi, F. E.; Sandaroos, R. *Inorganic Chemistry Commun.* **2020**, *122*, 108287.
<https://doi.org/10.1016/j.inoche.2020.108287>.
28. Tahmasbi, B.; Moradi, P.; Darab, M. *Nanoscale Advances*, **2024**, 7(26), 1932-1944.
<https://doi.org/10.1039/D3NA01087B>.
29. Ara, M.; Ghafari, H.; Ghanbar, N. *Colloid and interface science communications*, **2023**, *53*, 100704.
<https://doi.org/10.1016/j.colcom.2023.100704>.
30. Dehghani, F.; Sardarian, A.R.; Esmailpour, M. *J. Organometallic Chem.* **2013**, *743*, 87-96.
<https://doi.org/10.1016/j.jorganchem.2013.06.019>.
31. Tabaković, I.; Trkovnik, M.; Galijaš, D. *J. Electroanal. Chem.* **1978**, *86*, 241-244.
[https://doi.org/10.1016/S0022-0728\(78\)80373-8](https://doi.org/10.1016/S0022-0728(78)80373-8).
32. Jiang, Y.Y.; Liang, S.; Zeng, C.C.; Hu, L.M.; Sun, B.G. *Green Chem.* **2016**, *18*, 6311-6319.
<https://doi.org/10.1039/C6GC01970F>.
33. Wang, Y.; Qian, P.; Su, J. H.; Li, Y.; Bi, M.; Zha, Z.; Wang, Z. *Green Chem.* **2017**, *19*, 4769-4773.
<https://doi.org/10.1039/C7GC01989K>.
34. Frisch, M. J.; Trucks, G.W.; Schlegel, H.B.; Scuseria, G. E.; Robb, M.A.; Cheeseman, J. R.; Scalmani, G.; Barone, V.; Mennucci, B.; Petersson, G. A.; Nakatsuji, H.; Caricato, M. L.X.; Hratchian, H. P.; Izmaylov, A. F.; Bloino, J. G.; Zheng, Sonnenberg, J.L.; Hada, M.; Ehara, M.; Toyota, K.; Fukuda, R.; Hasegawa, J.; Ishida, M.; Nakajima, T.; Honda, Y. M.; Kitao, O.; Nakai, H.; Vreven, T.; Montgomery, J. A. J.; Peralta, J.E.; Ogliaro, F.; Bearpark, M.; Heyd, J. J.; Brothers, E.; Kudin, K. N.; Staroverov, V. N.; Kobayashi, R.; Normand, J.; Raghavachari, K.; Rendell, A.; Burant, J.C.; Iyengar, S.S.; Tomasi, J.; Cossi, M.; Rega, N.; Millam, J. M.; Klene, M.; Knox, J.E.; Cross, J. B.; Bakken, V.; Adamo, C.; Jaramillo, J.; Gomperts, R.; Stratmann, R.E.; Yazyev, O.; Austin, A. J.; Cammi, R.; Pomelli, C.; Ochterski, J. W.; Martin, R. L.; Morokuma, K.; Zakrzewski, V. G.; Voth, G. A.; Salvador, P.; Dannenberg, J. J.; Dapprich, S.; Daniels, A.D.; Farkas, O.; Foresman, J. B.; Ortiz, J.V.; Cioslowski, J.; Fox, D. J.; Gaussian 09, Revision E.01; Gaussian Inc.: Wallingford, CT, **2013**.
35. Mendoza-Huizar, L.H.; Rios Reyes, C.H. *J. Mex. Chem. Soc.* **2011**, *55*, 142-147.
<https://doi.org/10.29356/jmcs.v55i3.812>.
36. Piyanzina, I.; Minisini, B.; Tayurskii, D.; Bardeau, J.F. *J. Mol. Model.* **2015**, *21*, 34-38.
[https://doi.org/10.1016/0263-7855\(96\)00018-5](https://doi.org/10.1016/0263-7855(96)00018-5).
37. Ghanty, T.K.; Ghosh, S.K.A. *J. Phys. Chem.* **1996**, 100(30), 12295-12298.

- <https://doi.org/10.1021/jp960276m>.
38. Koopmans, T. *Physical*, 1933, 1, 104-113.
[https://doi.org/10.1016/S0031-8914\(34\)90011-2](https://doi.org/10.1016/S0031-8914(34)90011-2).
39. Dena, A.S. A.; Hassan, W. M. I. *Spectrochim. Acta Part A. Mol. Biomol. Spectrosc.* **2016**, 163, 108-114.
<https://doi.org/10.1016/j.saa.2016.03.030>.
40. Dena, A.S.A.; Muhammad, Z.A.; Hassan, W.M.I. *Chem. Pap.* **2019**, 73,2803-2812.
<https://doi.org/10.1007/s11696-019-00833-7>.
41. Muglu, H.; Kurt, B.Z.; Sonmez, F.; Guzel, E.; Cavus, M. S.; Yakan, H. J. *Phys. Chem. Solids.* **2022**, 164, 110618.
<https://doi.org/10.1016/j.jpcs.2022.110621>.
42. Cavus, M.S.; Yakan, H.; Ozorak, C.; Muglu, H.; Bakır, T. K. *Res. Chem. Intermed.* **2022**, 48, 1593-1613.
<https://doi.org/10.1007/s11164-022-04659-z>.
43. Muglu, H.; Akın, M.; Cavus, M.S.; Yakan, H.; Şaki, N.; Güzel, E. *Comput. Biol. Chem.* **2022**, 96, 107618.
<https://doi.org/10.1016/j.compbiolchem.2021.107618>
44. Muglu, H.; Yakan, H.; Misbah, A.G.A.; Cavus, M.S.; Bakır, T. K. *Res. Chem. Intermed.* **2021**, 47, 4985- 5005.
<https://doi.org/10.1007/s11164-021-04576-7>.
45. Henriksson, J.; Saue, T.; Norman. P. *J.Chem.Phys.* **2008**, 128, 024105.
<https://doi.org/10.1063/1.2816709>.
46. Mottishaw, J. D.; Erck, A. R.; Kramer, J. H.; Sun, H.; Koppang, M. J. *Chem. Educ.* **2015**, 92(11), 1846- 1852.
<https://doi.org/10.1021/ed5006344>
47. Ahmed, A.; Fatima, A.; Shakya, S.; Rahman, Q. I.; Ahmad, M.; Javed, S.; Ahmad, H. S. A. *Molecules*, **2022**, 27, 1724-1745.
<https://doi.org/10.3390/molecules27051724>.
48. Noury, S.; Krokidis, X.; Fuster, F.; Silvi, B. *Comput. Chem. (Oxford)* **1999**, 597– 604.
[https://doi.org/10.1016/S0097-8485\(99\)00039-X](https://doi.org/10.1016/S0097-8485(99)00039-X)
49. Becke, A.D.; Edgecombe, K.E. *J. Chem Physics*, **1990**, 5397-5403.
<https://doi.org/10.1063/1.458517>.
50. Mosmann, T. J. *Immunol Methods*, **1983**, 65, 53-63.
[https://doi.org/10.1016/0022-1759\(83\)90303-4](https://doi.org/10.1016/0022-1759(83)90303-4).
51. Dhiman, N.; Kaur, K.; Jaitak, V. *Bioorg. Med. Chem.* 2020, 28(15), 115599.
<https://doi.org/10.1016/j.bmc.2020.115599>
52. Verma, A.; Kaur, B.; Venugopal, S.; Wadhwa, P.; Sahu, S.; Kaur, P.; Kumar, D.; Sharma, A. *Chem. Biol. Drug Des.* 2022, 100(3), 419-442.
<https://doi.org/10.1111/cbdd.14103>
53. Kumar, Ch. N. S. S. P.; Parida, D. K.; Santhoshi, A.; Kota, A. K.; Sridhar, B.; Rao, V. J. *Med. Chem. Commun.*2011, 2, 486-492.
<https://doi.org/10.1039/C0MD00263A>
54. Popova, E. A.; Protas, A. V.; Trifonov, R. E. *Anticancer Agents Med Chem* 2018, 17(14), 1856-1868.
<https://doi.org/10.2174/1871520617666170327143148>
55. Trifonov, R. E.; Ostrovskii, V. A. *Int. J. Mol. Sci.* 2023, 24(24), 17190.
<https://doi.org/10.3390/ijms242417190>

56. Yu, Z.; Yin, Y.; Zhao, W.; Liu, J. Chen, F. Food Chem. **2012**, 135, 2078-2085.
<https://doi.org/10.1016/j.foodchem.2012.06.088>.

This paper is an open access article distributed under the terms of the Creative Commons Attribution (CC BY) license (<http://creativecommons.org/licenses/by/4.0/>)